Journal of Structural Geology, Vol. 10, No. 3, pp. 225 to 237, 1988
Printed in Great Britain

0191-8141/88 $03.00 + 0.00

Multiple fault sets and three-dimensional strain: theory and application

ROBERT W. KRANTZ

Department of Geosciences, The University of Arizona, Tucson, AZ 85721, U.S.A.

(*Received* 20 *August* 1986; *accepted in revised form* 10 *September* 1987)

Abstract—The widely accepted faulting theory of Anderson fails to explain three more coeval sets of faults or faults developed in a three-dimensional strain field. Reches has developed a model which suggests that four sets of faults, arranged in orthorhombic symmetry about the principal strain axes, are necessary to accommodate general, three-dimensional strain. This paper presents the odd-axis model, which recognizes certain geometric and kinematic relationships inherent in orthorhombic fault systems and in the Reches model and presents a practical method for decoding the strain significance of fault systems developed in three-dimensional strain fields. Both the odd-axis model and the Reches model are applied to an array of orthorhombic faults in the northern San Rafael Swell of central Utah with excellent agreement between predicted and observed geometric and kinematic parameters.

INTRODUCTION

MOST geologists are quite familiar with the idea that faults may develop in conjugate pairs, where each of the two sets in the pair represents a number of parallel faults. Since the landmark work of Anderson (1951), structural geology texts have described conjugate faults, which intersect in the intermediate strain and stress directions, as the two potential orientations for developing faults. The plane perpendicular to the intermediate axis contains both the maximum and minimum strain and stress directions and the fault slip vectors (Ramsay 1967, Hobbs *et al.* 1976). Many field and laboratory investigations have successfully applied conjugate fault theory to the extent that many geologists accept it as universal. Recent work, however, suggests that conjugate faults are only a special case of more general fault deformation.

Experimental (Oertel 1965) and field (Aydin & Reches 1977, Krantz 1986) observations have revealed fault systems with four sets of coeval faults, arranged in orthorhombic symmetry. All examples were interpreted as faulting in response to three-dimensional strain, and none could be explained in the context of conjugate faults.

Both the slip model of Reches (1978, 1983) and the odd-axis model (this paper) represent attempts to explain multiple fault sets in the context of three-dimensional, or true triaxial, strain fields. Both methods also assume irrotational strain. These models suggest that fault geometry is in part a function of the ratios of the principal strains, especially the relative magnitude of the intermediate strain, and that four sets of faults are necessary in the general case. Conjugate faults are interpreted as a special case consistent with both models.

To date, Reches' slip model has been tested only by laboratory deformation experiments, with the results in good agreement with the model (Aydin & Reches 1982, Reches & Dieterich 1983). The Chimney Rock fault array, a system of normal faults in the northern San Rafael Swell of central Utah, presents an outstanding opportunity to apply and test both models in the field (Krantz 1986). The excellent exposure at Chimney Rock allows for independent calculations of the principal strains which can be compared to kinematic parameters predicted by the models based on fault geometry.

THE SLIP MODEL

The odd-axis analysis is based in part on the results of the slip model of faulting derived by Reches (1978, 1983), and therefore the slip model will first be reviewed briefly.

Unlike many fault models that describe the failure of coherent isotropic materials, the slip model assumes that the body to be deformed contains many pre-existing, randomly oriented planes of discontinuity. Reches (1983) proposed that, within a given strain field, the surfaces along which slip will first take place are those that are most favorably oriented with respect to the principal strain axes. The slip model assumes that failure on each individual surface follows Coulomb frictional behavior and that the strain field is irrotational and of constant volume.

Reches applied tensor analysis to identify the preferred fault orientations and slip vectors. His analysis proceeded by simultaneous minimizing of the differential stress and the energy dissipation necessary to initiate slip.

The preferred orientations are derived as functions of the principal extensions, ε_i, where $\varepsilon_x > \varepsilon_y > \varepsilon_z$, and the angle of internal friction, ϕ. Reches defines the ratio of intermediate to minimum extension as k, where

$$k = \frac{\varepsilon_y}{\varepsilon_z}. \quad (1)$$

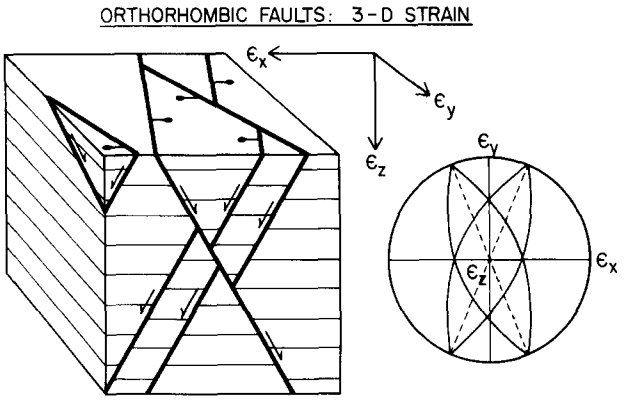

Fig. 1. Block diagram and stereonet of orthorhombic faults. The faults are arranged in four sets symmetrical about the principal strain axes.

k may range from $-\frac{1}{2}$ to 1, with plane strain occurring where $k = 0$.

The preferred fault orientations are presented as stereonet plots and as sets of equations for direction cosines of poles to faults (Reches 1983 and Appendix A, this paper). Four sets of faults, arranged in orthorhombic symmetry about the principal strain axes, are predicted for three-dimensional strain (Fig. 1).

THE ODD-AXIS MODEL

The odd-axis model determines the principal strain axes and their relative magnitudes from orientations of fault planes and slip vectors. Only the strain accommodated by slip along the faults is considered. It is assumed that the strain is irrotational. Furthermore, the derivation of the strain equations below assumes that slip is equally distributed among the fault sets and the individual faults.

The foundation of the odd-axis model is the recognition of the 'odd' axis: the one principal strain axis with sign opposite the other two, assuming a three-dimensional, constant volume strain field. If one principal extension (strain) is positive and the other two are negative, then the ε_x axis is the odd axis. If one principal extension is negative and the other two are positive, then the ε_z axis is the odd axis. The intermediate axis, ε_y, and the similar axis share the same sign. The similar axis must be ε_z where the odd axis is ε_x, and vice versa.

Interpreting the slip model

By applying the odd-axis concept to the slip model, two important geometric relationships emerge. The first relates the orientations of the preferred faults to different values of k. The second relates the orientation of the slip vector predicted for a fault set to the pole to that set and the odd axis.

Figure 2(a) shows a pair of conjugate faults and a plane-strain field with $k = 0$. No odd axis can be defined. With ε_z oriented vertically, these are normal faults. The acute angle between the faults is 2θ, where

$$\theta = \frac{90° - \phi}{2} \quad \text{(Anderson 1951).} \tag{2}$$

Figure 2(b) shows a three-dimensional strain field, with a relatively small amount of positive extension in the ε_y direction, so that $-\frac{1}{2} < k < 0$. The ε_z axis must now be the odd axis. The slip model predicts four sets of normal faults, arranged in two pairs. The faults of each pair intersect in the plane containing the intermediate and similar axes. The acute angle between the faults of each pair is $2\theta'$. For $k < 0$, θ' is the angle between any fault plane and the odd axis (ε_z). θ' is also the complement of the angle between the pole to any of the fault sets and ε_z:

$$\begin{aligned}\theta' &= 90° - \cos^{-1} N_z \\ &= 90° - \cos^{-1}[(\sqrt{2}/2)(1 - \sin\phi)^{1/2}],\end{aligned} \tag{3}$$

where N_z is the cosine of the angle between the fault pole and the ε_z axis (Appendix A).

Equation (3) can be reduced so that

$$\theta' = \frac{90° - \phi}{2} = \theta. \tag{3a}$$

Thus the angular relationship between the faults of each orthorhombic pair is the same as for conjugate pairs. θ' and θ are controlled by the friction angle, ϕ, and are independent of k.

The angular relationship between the strikes of each pair, as measured in the intermediate–similar plane, however, is a function of the intermediate to minimum strain ratio (k). For strain fields with successively greater relative magnitudes of extension in the ε_y direction, the strikes of the predicted fault pairs are different. As shown in the rest of Fig. 2, the range of predicted faults can be represented by a rotation of the fault pairs about the vertical ε_z or odd axis.

Similarly, the range of predicted reverse fault set orientations can be represented by a rotation of fault pairs about the ε_x or odd axis as k ranges from zero (plane strain) to unity (axially-symmetric constriction) and back to zero (plane strain) (Fig. 3). Figures 2 and 3 demonstrate how conjugate faults represent a special case of more general fault set geometries.

The slip model also reveals a specific geometric relationship between the slip vectors predicted for the preferred faults and the odd axis. For irrotational plane strain, the slip vectors are defined by the intersections of the conjugate fault planes and the $\varepsilon_z - \varepsilon_x$ plane (Hobbs *et al.* 1976). For orthorhombic faults, none of the slip vectors lie in any of the principal strain planes. Instead, the slip vector for each of the preferred fault sets is defined by the intersection of the fault plane and a second plane containing the pole to the fault and the odd axis. The slip vector, fault pole and odd axis are coplanar, and with the odd axis oriented vertically, the slip vector must rake 90° (pure dip-slip) (Fig. 4). Horizontal odd axes require oblique slip. Appendix B presents a proof of the coplanar relationship of slip vector, fault pole and odd axis, based on slip model orientation equations.

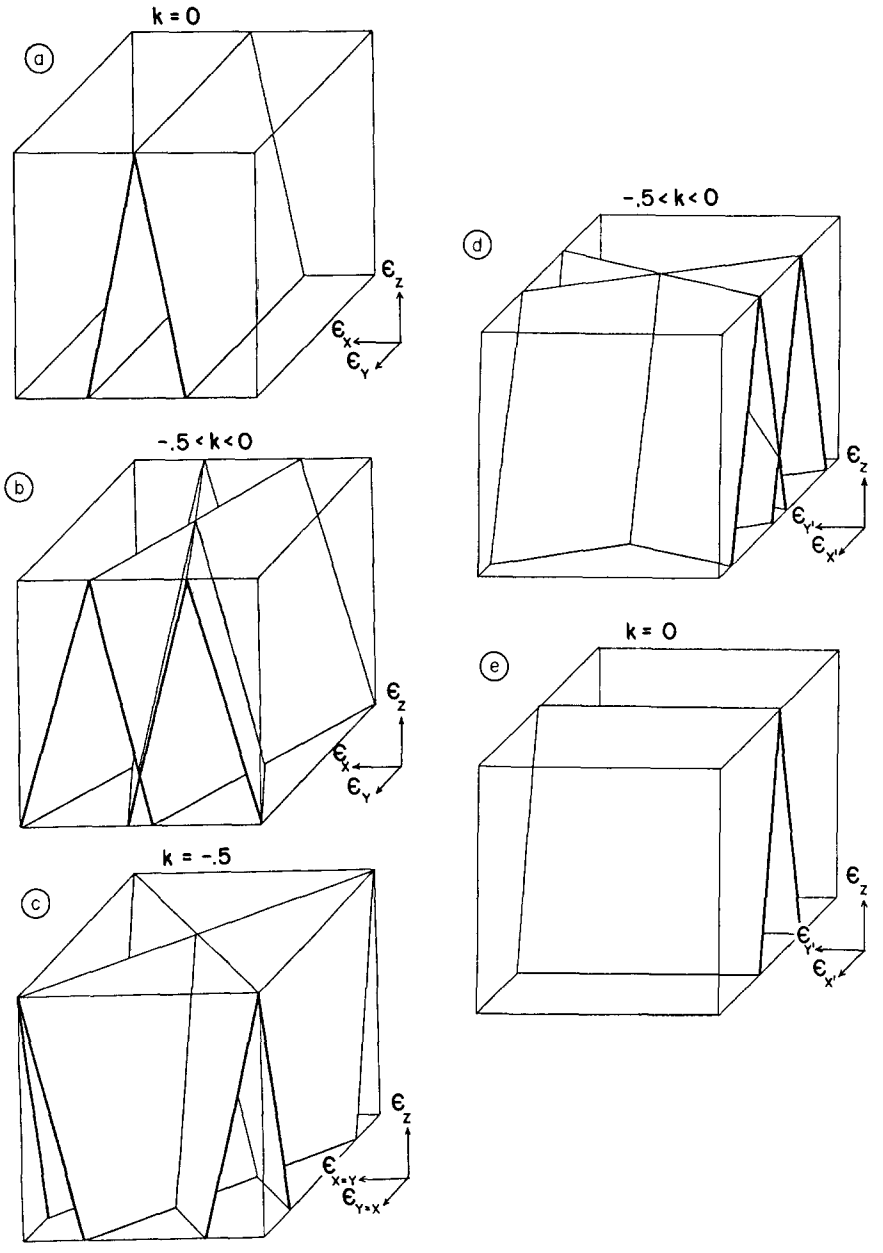

Fig. 2. Series of block diagrams showing sets of normal faults predicted for values of k ranging from 0 to $-\frac{1}{2}$. The range of predicted fault set orientations can be represented by a rotation of fault pairs about the vertical odd axis, ε_z. Note that in (d) and (e) the relative extension in the original intermediate strain direction has become greater than that of the original maximum direction so that ε_x becomes $\varepsilon_{y'}$ and ε_y becomes $\varepsilon_{x'}$.

Odd-axis construction

Because the odd axis lies in the planes defined by the poles to the faults and the slip vectors, a simple stereonet construction can solve for the odd axis (Fig. 5). The plane containing each fault pole and associated slip vector is represented as a great circle. The common intersection of these planes, or average of intersections, is the odd axis. This construction is directly analogous to that proposed by Arthaud (1969). For a large number of data pairs, statistical means for clusters of fault poles and associated striae provide the basis for a neater construction.

The other two principal strains must lie in a plane perpendicular to the odd axis (Fig. 5). The similar axis, which will be either the ε_z or the ε_x axis, will bisect the acute angle between the clusters of great circles. The intermediate axis will bisect the obtuse angle, 90° from both the odd and similar axes.

Upon defining the orientation of the odd axis, one can distinguish whether it is the ε_z or ε_x axis on the basis of additional structural geologic information. Fault systems with extension in the odd axis direction imply that ε_x is the odd axis. Conversely, shortening in the odd-axis directions suggests that ε_z is the odd axis.

KINEMATICS OF ORTHORHOMBIC FAULTS

The odd-axis concept can be applied to orthorhombic fault geometry to decode the strain significance of such systems. The geometric relationships between fault

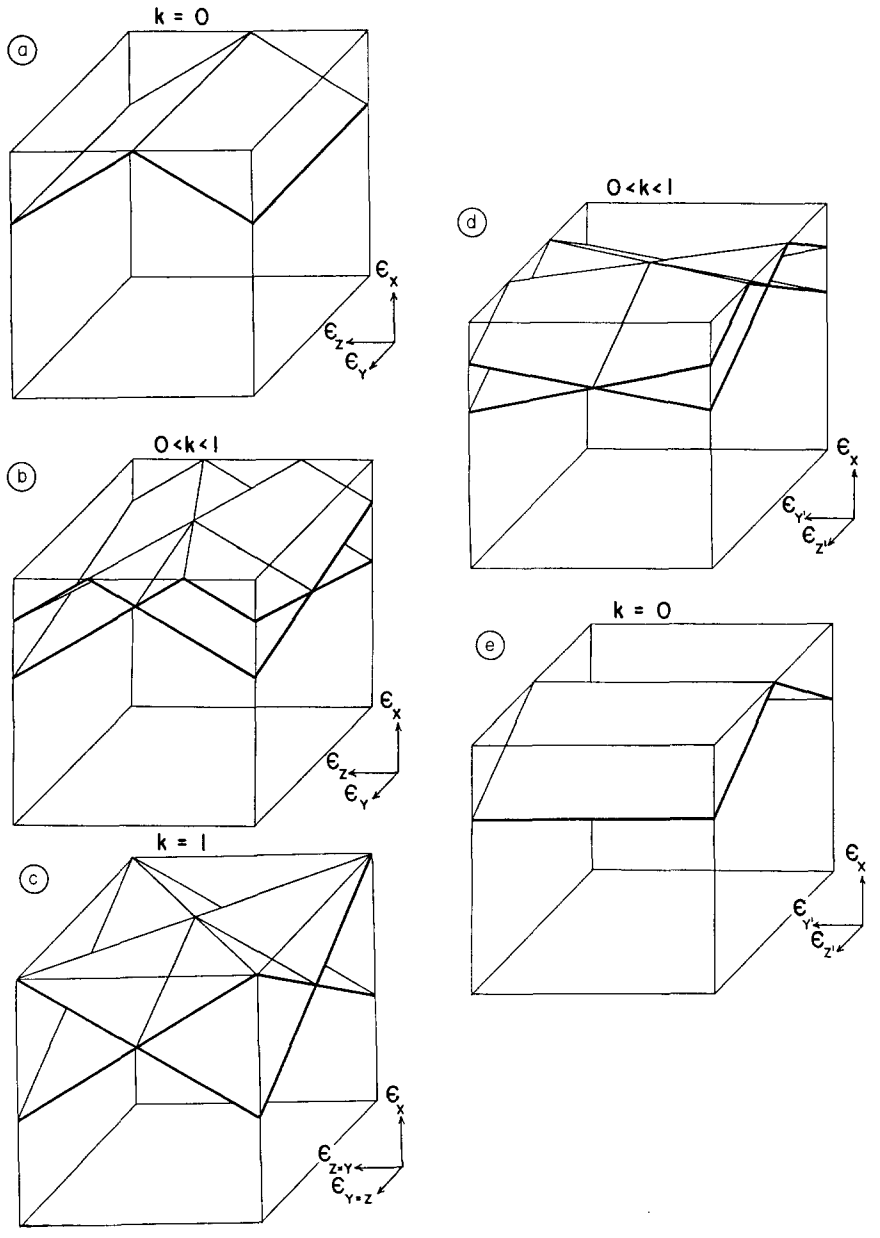

Fig. 3. Series of block diagrams showing sets of reverse faults predicted for values of k ranging from 0 to 1. The range of predicted fault set orientations can be represented by a rotation of fault pairs about the vertical odd axis, ε_x. Note that in (d) and (e) the relative amount of shortening in the original intermediate direction has become greater than that of the original minimum direction so that ε_z becomes $\varepsilon_{y'}$ and ε_y becomes $\varepsilon_{z'}$.

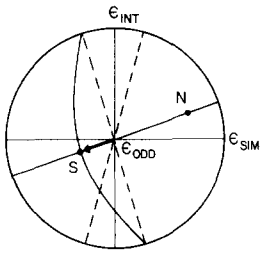

Fig. 4. Stereonet illustrating the coplanar relationship of fault pole (N), slip vector (S) and odd axis. Also shown are the fault plane defined by the pole (solid), the common strikes for the pairs of orthorhombic faults (dashed), and the similar and intermediate axes.

planes, slip vectors and the principal strain axes allow for determination of principal strain magnitudes and ratios from fault set geometry. The model assumes both constant volume and irrotational strain, and can accommodate both finite and infinitesimal strains. For some fault systems, strain ratio calculations are especially simple.

The derivation is based on the symmetry of orthorhombic systems and assumes an equal distribution of strain among the four fault sets as well as among the faults of one set. Thus the strain of one fault set will represent the other three.

The derivation begins by calculating the extensions in each of the principal directions as functions of the spacing between the parallel faults of one set, the average magnitude of fault slip and the orientation of the plane representing the fault set relative to the principal strain

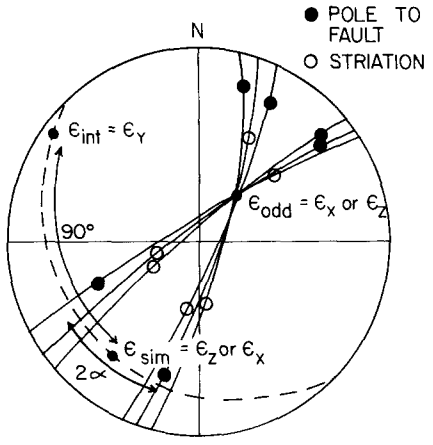

Fig. 5. Example of an odd-axis construction. Each great circle is defined by a fault pole and striation on that fault. The common intersection of the great circles is the odd axis, which must be either ε_x or ε_z. The other two principal strains must be located on the plane perpendicular to the odd axis (dashed). The similar axis, ε_z or ε_x, bisects the acute angle between the clusters of great circles. The intermediate axis, ε_y, bisects the obtuse angle. 2α is the acute angle between the clusters measured in the intermediate-similar plane.

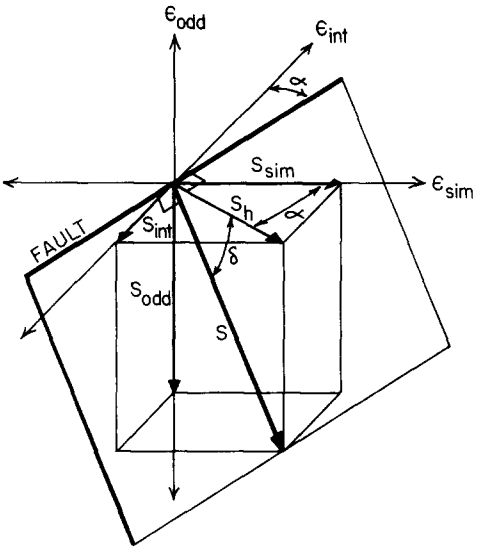

Fig. 6. Three-dimensional strain field with vertical odd axis and section of an orthorhombic fault. α is the angle between the fault strike and the intermediate axis, and δ is the dip of the fault. The slip vector, **S**, is resolved into a horizontal component, S_h, and components parallel to the principal strain axes.

axes. This orientation is expressed as α, the angle between the intermediate axis and the strike of the fault (set) as measured in the intermediate–similar plane, and δ, the dip of the fault measured from the intermediate–similar plane (Fig. 6). In the odd-axis construction (Fig. 5), the angle between the clusters of great circles, measured in the intermediate–similar plane, is 2α.

Extension is defined as the change in length over the initial length, or

$$\varepsilon_i = \frac{\Delta l_i}{l_i} = \frac{\Delta l_i}{l_i' - \Delta l_i}, \tag{4}$$

where l_i is the initial length, l_i' is the final length, and Δl_i is the change in length, all in the i-direction, so that

$$l_i' = l_i + \Delta l_i. \tag{5}$$

For an orthorhombic fault array, the change in length in any one of the principal directions due to faulting is given by

$$\Delta l_i = n_i S_i, \tag{6}$$

where n_i is the number of faults encountered in the i-direction and S_i is the component of average slip in the i-direction.

For one fault, the components of slip parallel to the principal strain direction (Fig. 6) are simple functions of the fault strike and the average slip, S (positive for normal slip), and are given by

$$S_{int} = S \sin \alpha \cos \delta, \tag{7}$$

$$S_{sim} = S \cos \alpha \cos \delta \tag{8}$$

and

$$S_{odd} = S \sin \delta. \tag{9}$$

The number of faults (of one set) encountered in the i-direction is given by

$$n_i = \frac{l_i'}{d_i}, \tag{10}$$

where d_i is the average distance between the parallel faults in the i-direction. This distance is a function of the average fault spacing, d, measured perpendicular to the fault planes, and of α and δ. Interfault distances in the three principal directions are given by

$$d_{int} = \frac{d}{\sin \alpha \sin \delta}, \tag{11}$$

$$d_{sim} = \frac{d}{\cos \alpha \sin \delta} \tag{12}$$

and

$$d_{odd} = \frac{d}{\cos \delta}. \tag{13}$$

Substituting equations (11), (12) and (13) into equation (10) yields

$$n_{int} = \frac{l_{int}' \sin \alpha \sin \delta}{d}, \tag{14}$$

$$n_{sim} = \frac{l_{sim}' \cos \alpha \sin \delta}{d} \tag{15}$$

and

$$n_{odd} = \frac{l_{odd}' \cos \delta}{d}. \tag{16}$$

The change in length in the principal directions is derived by substituting equations (7) and (14), (8) and (15), and (9) and (16) into equation (6):

$$\Delta l_{int} = \frac{l_{int}' S}{d} \sin^2 \alpha \sin \delta \cos \delta = \frac{l_{int}' R}{2} \sin^2 \alpha \sin 2\delta, \tag{17}$$

$$\Delta l_{sim} = \frac{l'_{sim}S}{d} \cos^2 \alpha \sin \delta \cos \delta = \frac{l'_{sim}R}{2} \cos^2 \alpha \sin 2\delta \tag{18}$$

and

$$\Delta l_{odd} = \frac{l'_{odd}S}{d} \sin \delta \cos \delta = \frac{l'_{odd}R}{2} \sin 2\delta, \tag{19}$$

where

$$R = \frac{S}{d}. \tag{20}$$

R represents the ratio of fault slip to fault spacing.

The equations for extension in the principal directions due to one fault set are obtained by substituting equations (17), (18) and (19) into equation (4):

$$\varepsilon_{int} = \frac{(l'_{int}R/2) \sin^2 \alpha \sin 2\delta}{l'_{int} - (l'_{int}R/2) \sin^2 \alpha \sin 2\delta} = \frac{(R/2) \sin^2 \alpha \sin 2\delta}{1 - (R/2) \sin^2 \alpha \sin 2\delta}, \tag{21}$$

$$\varepsilon_{sim} = \frac{(l'_{sim}R/2) \cos^2 \alpha \sin 2\delta}{l'_{sim} - (l'_{sim}R/2) \cos^2 \alpha \sin 2\delta} = \frac{(R/2) \cos^2 \alpha \sin 2\delta}{1 - (R/2) \cos^2 \alpha \sin 2\delta} \tag{22}$$

and

$$\varepsilon_{odd} = \frac{-(l'_{odd}R/2) \sin 2\delta}{l'_{odd} - (l'_{odd}R/2) \sin 2\delta} = \frac{-(R/2) \sin 2\delta}{1 - (R/2) \sin 2\delta}. \tag{23}$$

The negative sign inserted in equation (23) signifies the opposite sense of strain in the odd-axis direction. These equations express the principal extensions as functions of the fault strike and dip (as measured with the odd axis vertical) and the ratio of fault slip to fault spacing. The final length, l'_i, has been factored out. The principal extensions produced by four sets of faults would require multiplying equations (21)–(23) by a factor of four, assuming true orthorhombic symmetry and equal distribution of strain.

Equations (21)–(23) can now be used to determine the ratios of principal extension:

$$\frac{\varepsilon_{int}}{\varepsilon_{sim}} = \tan^2 \alpha \frac{(1 - (R/2) \cos^2 \alpha \sin 2\delta)}{(1 - (R/2) \sin^2 \alpha \sin 2\delta)}, \tag{24}$$

$$\frac{\varepsilon_{int}}{\varepsilon_{odd}} = -\sin^2 \alpha \frac{(1 - (R/2) \sin 2\delta)}{(1 - (R/2) \sin^2 \alpha \sin 2\delta)} \tag{25}$$

and

$$\frac{\varepsilon_{sim}}{\varepsilon_{odd}} = -\cos^2 \alpha \frac{(1 - (R/2) \sin 2\delta)}{(1 - (R/2) \cos^2 \alpha \sin 2\delta)}. \tag{26}$$

These last equations express the ratios of principal extensions as functions of fault strike and dip (as measured with the odd axis vertical) and the ratio of fault slip to fault spacing. Because these equations describe ratios of strain, the number of fault sets involved is immaterial. Furthermore, the equations are applicable to fault systems with unequal development of faults among the four possible sets.

Because equations (24)–(26) were derived without restrictions on the magnitude of fault slip, they are valid for both finite and infinitesimal strains. The critical parameter is not the magnitude of strain but the ratio of average fault slip to average fault spacing.

For fault systems where the ratio of fault slip to fault spacing, R, is small, the extension ratio equations can be greatly simplified. As R approaches zero, the fractional portion in each of equations (24)–(26) approaches unity, so that

$$\frac{\varepsilon_{int}}{\varepsilon_{sim}} \simeq \tan^2 \alpha, \tag{27}$$

$$\frac{\varepsilon_{int}}{\varepsilon_{odd}} \simeq -\sin^2 \alpha \tag{28}$$

and

$$\frac{\varepsilon_{sim}}{\varepsilon_{odd}} \simeq -\cos^2 \alpha. \tag{29}$$

The accuracy of the simplified equations (27)–(29) relative to the complete equations (24)–(26) can be estimated by calculating the ratio of the complete equation to the simplified equation, where 1.0 represents total accuracy. Figure 7 shows a series of curves that represent equal values of the ratio of equation (24) to equation (27) for various values of α and R. ϕ is assumed to be 30°, and the curves are identical for δ values of 30 or 60°.

As seen in Fig. 7, the accuracy of equation (27) increases as α increases or as R decreases. Equivalent plots for equations (25) and (28) and equations (26) and (29) would show similar results. In general, for R values less than 0.1, equations (27)–(29) will yield errors of 4% or less for all values of α.

Although the fault dip, δ, appears in equations (24)–(26), it factors out of the simplified extension ratio equations (27)–(29). These equations use only the fault strike, α, which can be measured from the odd-axis construction (Fig. 5) or from field exposures or maps of

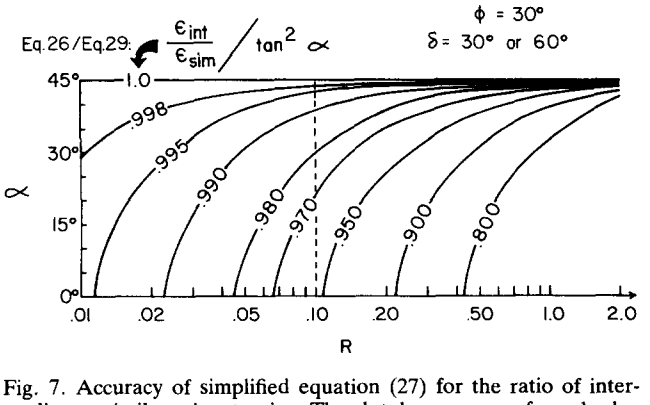

Fig. 7. Accuracy of simplified equation (27) for the ratio of intermediate to similar axis extension. The plot shows curves of equal value of the ratio of equation (27) to equation (24) as functions of R and α. 1.0 represents complete accuracy. ϕ = 30° and δ = 30 or 60°. For $R \leq 0.1$, equation (27) yields values accurate to 96% or better for all values of α.

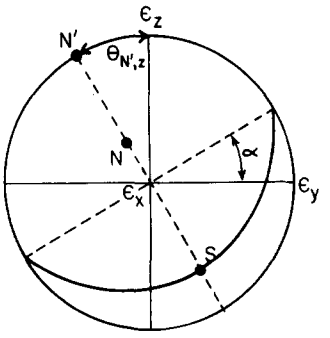

Fig. 8. Stereonet plot illustrating the relationships of the fault pole, **N**, the horizontal projection of the fault pole, **N'**, the slip vector, **S** and the principal strains. The fault defined by the pole strikes at an angle α from the ε_y axis. **N'** trends at an angle $\theta_{N',z}$ from the ε_x axis. $\theta_{N',z} = \alpha$.

fault systems with observed dip-slip vectors. Equations (27)–(29) should be restricted to fault systems with R values less than 0.1, which implies finite strains of a few per cent or less.

Equations (27)–(29) can also be compared with those of Reches' slip model. For $k > 0$, the similar axis is ε_z and equation (27) becomes

$$\frac{\varepsilon_{\text{int}}}{\varepsilon_{\text{sim}}} = \frac{\varepsilon_y}{\varepsilon_z} = \tan^2 \alpha. \tag{30}$$

As shown stereographically in Fig. 8, **N'**, the horizontal projection of the fault pole **N**, lies at an angle $\theta_{N',z}$ from the ε_z axis, and $\theta_{N',z} = \alpha$. Thus

$$\tan^2 \alpha = \tan^2 \theta_{N',z} = \frac{\sin^2 \theta_{N',z}}{\cos^2 \theta_{N',z}} = \frac{1 - \cos^2 \theta_{N',z}}{\cos^2 \theta_{N',z}}. \tag{31}$$

Using direction cosine notation ($\cos \theta_{A,i} \equiv A_i$), equation (31) becomes

$$\tan^2 \alpha = \frac{1 - (N'_z)^2}{(N'_z)^2}. \tag{32}$$

Substituting

$$N'_z = \frac{N_z}{(1 - N_x^2)^{1/2}} \tag{33}$$

into equation (31) yields

$$\tan^2 \alpha = \frac{1 - N_x^2 - N_z^2}{N_z^2}. \tag{34}$$

Finally, substituting the equations of the slip model for $k > 0$ for N_x and N_z (Reches 1983 and Appendix A) yields

$$\tan^2 \alpha = \frac{1 - \frac{1}{2}(1 + \sin \phi) - \frac{1}{2}(1/(1 + k))(1 - \sin \phi)}{\frac{1}{2}(1/(1 + k))(1 - \sin \phi)}, \tag{35}$$

which reduces to

$$\tan^2 \alpha = \frac{1 - (1/(1 + k))}{1/(1 + k)} = \frac{1 + k - 1}{1} = k. \tag{36}$$

Therefore,

$$\frac{\varepsilon_y}{\varepsilon_z} = \tan^2 \alpha = k, \tag{37}$$

which is the relationship defined by the slip model (Reches 1983).

A similar derivation for $k < 0$ and ε_z as the odd axis yields $\varepsilon_y/\varepsilon_z = k$ from equation (28), demonstrating that the kinematic implications of the odd-axis model and the slip model are compatible, at least for small values of R.

In general, both the odd-axis model and the slip model are most appropriate for fault systems where mechanical anisotropies and other structural complications are minimal, and where fault set geometry accurately reflects the finite strain field. As the magnitude of fault slip and the value of R grow larger, these conditions become more unlikely and fault plane or slip vector orientations can no longer be predicted accurately. Systems produced by superimposed episodes of faulting or reactivation of pre-existing faults may present geometric and kinematic patterns that cannot be understood in the context of simple orthorhombic or conjugate faulting.

THE CHIMNEY ROCK FAULT ARRAY

Together, the odd-axis model and the slip model of Reches (1983) offer a complementary theoretical context for analyzing fault patterns and strain fields. The practical value of these models can best be appreciated when applied to a system of orthorhombic faults in the field. The Chimney Rock fault array of central Utah contains four sets of faults arranged in orthorhombic symmetry. With nearly complete exposure, the Chimney Rock area allows for independent measure of principal strains and ratios, providing the basis for a quantitative test of the fault models.

The study area

The Chimney Rock fault array covers 25 km^2 of the northern San Rafael Swell of central Utah (Gilluly 1928) (Fig. 9). Ten major normal faults, traceable along strike for 1–3 km, and 30–40 minor faults displace the Jurassic Navajo Sandstone and overlying Carmel Formation (Orkid 1954, 1955, Cass 1955). Maximum observed vertical separation was 33 m.

Degree and completeness of exposure in the area are excellent. Fault-line scarps, developed in the uppermost Navajo Sandstone, present hundreds of meters of polished and striated fault surface (Fig. 10). Elsewhere, offset marker beds in the lower Carmel Formation tightly constrain fault location. Vertical separation can be measured directly where the Navajo–Carmel contact is exposed adjacent to the fault in both footwall and hangingwall (Fig. 11). In other locations, the distinctive and consistent stratigraphy of the lower Carmel Formation provides for ready separation calculations.

Located in the interior of the San Rafael Swell, the study area contains no major or minor complicating structures. Bedding dips 6° ± 2° throughout the area.

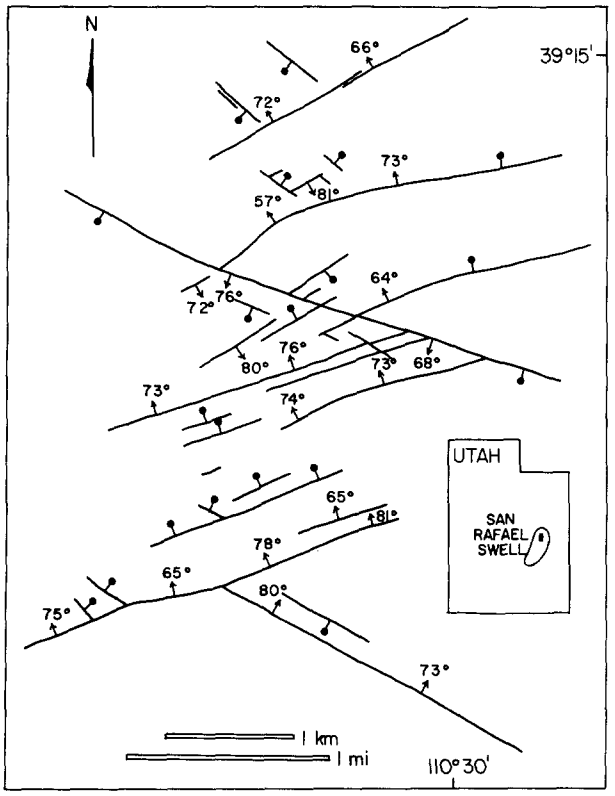

Fig. 9. Simplified map of the Chimney Rock fault array, located in the northern San Rafael Swell of central Utah. Ten major normal faults can be traced along strike for 1 km or more.

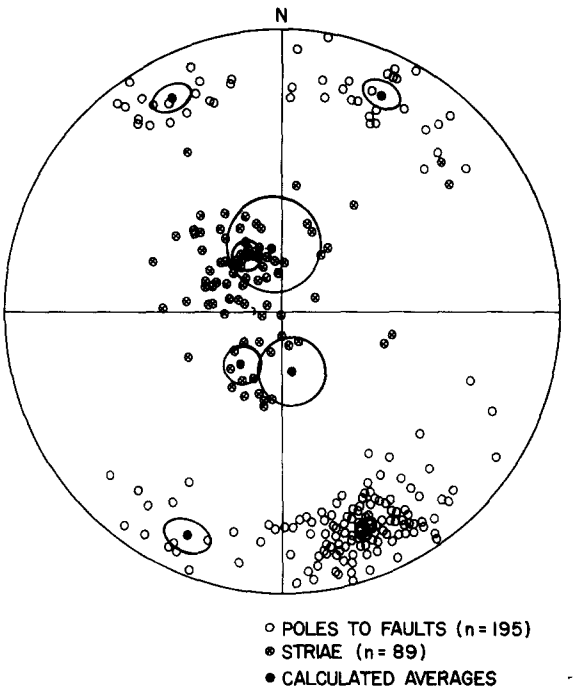

Fig. 12. Stereonet of poles to fault surfaces, striations, Fisher mean orientations and 95% confidence circles for the Chimney Rock array. The fault poles and striations define four sets in orthorhombic symmetry.

Fault geometry

As seen both in map pattern (Fig. 9) and stereographically (Fig. 12), the faults at Chimney Rock clearly define four sets: a pair striking west–northwest with one set dipping to the northeast and the other to the southwest, and a pair striking east–northeast with one set dipping to the northwest and the other to the southeast. Fault dips range from 55 to 85° and average 72°. Figure 12 shows the clusters of fault poles and striations along with the Fisher statistical mean and confidence circle for each cluster.

These orientations define an orthorhombic symmetry about axes nearly north–south, east–west and vertical. Mutual cross-cutting relationships between the four sets require coeval development of all faults. Thus the Chimney Rock faults comprise a true orthorhombic system.

The Chimney Rock fault array deviates from the ideal orthorhombic system in one respect. Both the map (Fig. 9) and the stereonet (Fig. 12) display a preponderance of northwest-dipping faults. This discrepancy will be addressed below.

Calculating observed principal strain values

The excellent and complete exposure at Chimney Rock allows accurate calculation of the principal strains. Testing the fault models requires a comparison of observed and predicted geometric and kinematic parameters. Testing also involves reconciling the calculated principal strain axes with the fault set symmetry axes, and evaluating the unequal distribution of faults among the four sets.

Figure 13 shows a map of vertical separations measured along the faults. Separation ranges from zero at fault terminations to a maximum of 33 m. Some faults can be traced from termination to termination along strike. Horizontal gradients of separation range from 3 to 30 m km^{-1} and average 15 m km^{-1}.

Because of the symmetry of fault sets about the north–south, east–west and vertical directions, these must be the principal strain axes. Furthermore, for an array of normal faults with dip-slip displacement, the horizontal principal strains must be extensional. Thus for Chimney Rock, ε_x is north–south, ε_y is east–west and ε_z is vertical.

A series of evenly-spaced transects were measured parallel to ε_x (19 transects) and to ε_y (26 transects). Each transect summed the components of fault slip parallel to the transect direction. Each component calculation was based on fault strike, fault dip and vertical separation at the point where the transect intersects a fault. Vertical strain (ε_z) was calculated from the other two assuming constant volume deformation.

Table 1 lists the average and maximum values calculated for the principal strains. All of the extension magnitudes are less than 0.01 and are therefore in the range of infinitesimal strain. The non-zero value of ε_y expresses the three-dimensional nature of the strain field, with positive extension in the intermediate strain direction. The maximum ε_x value of 0.0066 occurred in the center of the fault system, and ε_x values decreased systematically to both the east and west. Although east–northeast-striking faults dominate in number, the ε_x

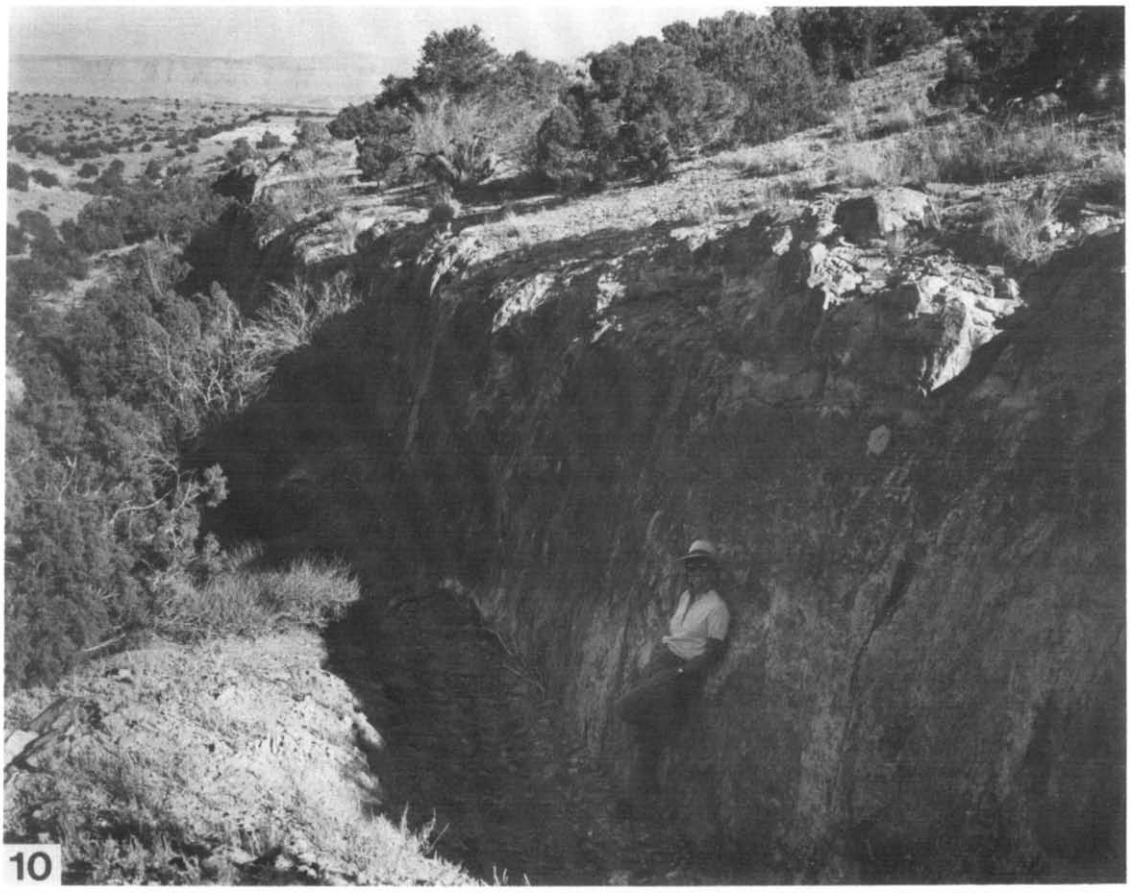

Fig. 10. Photograph of fault-line scarp at Chimney Rock, developed in the uppermost Navajo Sandstone. Net slip on this fault ranges from 7 m in the foreground to 13 m in the background.

Fig. 11. Photograph of 3 m fault-line scarp at Chimney Rock. The geologist is standing on the upper contact of the Navajo Sandstone, which is displaced above her head on the left.

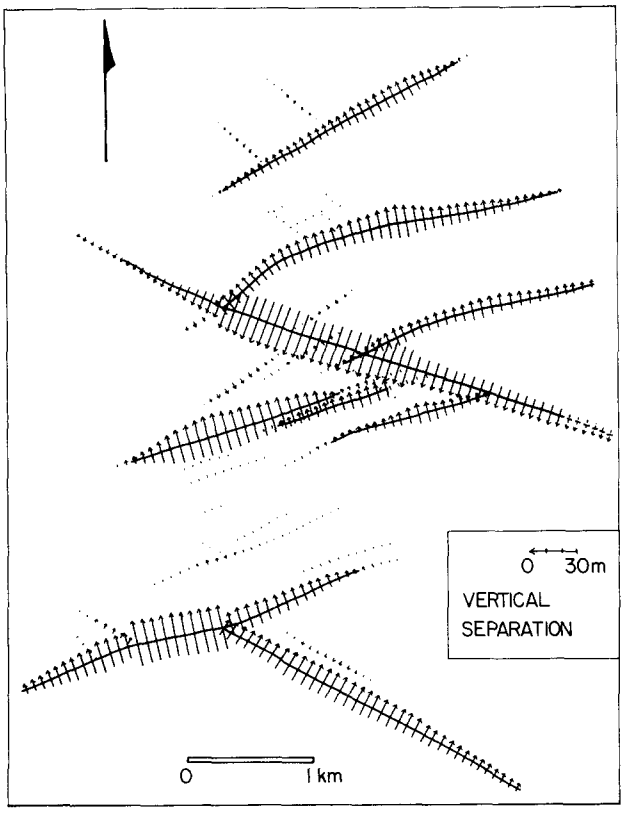

Fig. 13. Map of the Chimney Rock fault array showing patterns of fault slip measured in the field. Arrows point toward the hangingwall with lengths proportional to the magnitude of vertical separation. Many faults can be traced from maximum separation to termination(s).

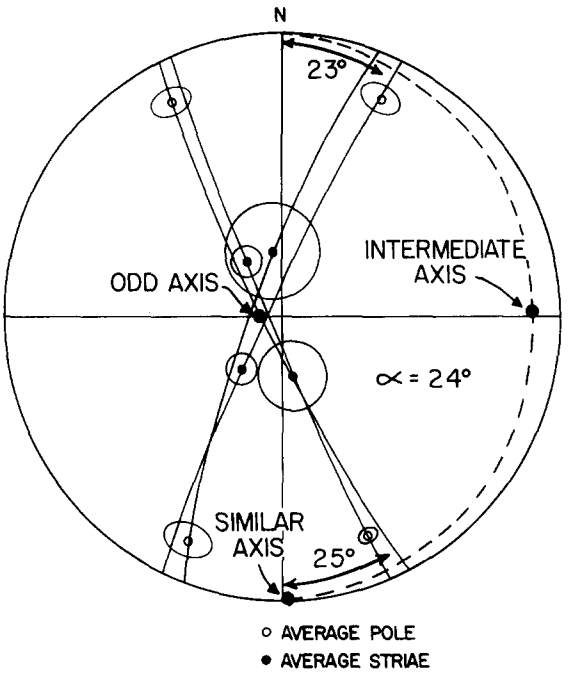

Fig. 14. Odd-axis construction for Chimney Rock using the mean orientations of fault sets and striations given in Fig. 12. The odd axis plunges steeply to the west, perpendicular to bedding. α is 24°.

transects from the center of the fault system contained zero net east–west strain. This suggests that ε_x is indeed north–south and that horizontal strain is equally distributed among the fault sets. ε_y values were less regular, with variable magnitudes from north to south across the array. The average intermediate extension is 0.0007.

Applying the fault models

The mean directions of fault pole and striation sets can be used for an odd-axis construction (Fig. 14). The great circles connecting the mean pole of each fault set and associated striation mean intersect in a number of points clustered about a line plunging approximately 84° to the west. This line is the odd axis and is perpendicular to bedding. The other two principal strains must be bedding-parallel.

The similar and intermediate axes are located on the plane perpendicular to the odd axis (Fig. 14). The intermediate axis bisects the obtuse angle between the great circles and the similar axis bisects the acute angle.

Table 1. Observed values of principal extension calculated from field data for the Chimney Rock fault array

	Average	Maximum
ε_x(north–south)	0.0041 ± 0.0018	0.0066
ε_y(east–west)	0.0007 ± 0.0004	0.0012
ε_z(vertical)	-0.0048 ± 0.0022	−0.0078

For Chimney Rock, the similar and intermediate axes trend only 1° counterclockwise from north–south and east–west, respectively; α, one-half the acute angle, is 24°.

Because the Chimney Rock array contains only normal faults, the near-vertical odd axis must be ε_z, the principal shortening axis. The other two axes, which both have sign opposite to that of the odd axis, must be extensional. The similar axis, ε_x, and the intermediate axis, ε_y, match the sense of strain revealed in the observed strain calculations above. The orientations of the constructed principal strains nearly match those used above, and are virtually identical after correcting for the eastward dip of bedding.

To apply the slip model, fault poles and associated striations must first be corrected for tilt and declination so that principal strains lie north–south, east–west and vertical on the stereonet. All of the poles are then reflected into the northeast quadrant using rules of orthorhombic symmetry (Reches 1983) (Fig. 15). The striations associated with each pole reflect accordingly.

For Chimney Rock, the reflected fault poles define a cluster with a Fisher mean trending 024° and plunging 18°. On the fault plane defined by the mean pole, the mean striation direction is very nearly dip-slip. The maximum of the contoured striations lies exactly down dip as the odd-axis model predicts.

Figure 16 shows the mean reflected fault pole plotted on the slip model net for normal faults, $k < 0$ (Reches 1983). The slip model predicts $k = -0.16 \pm 0.05$, using the confidence circle of the mean pole to set the error limits.

Before using the odd-axis model equations to determine the ratios of principal extension, R, the ratio of

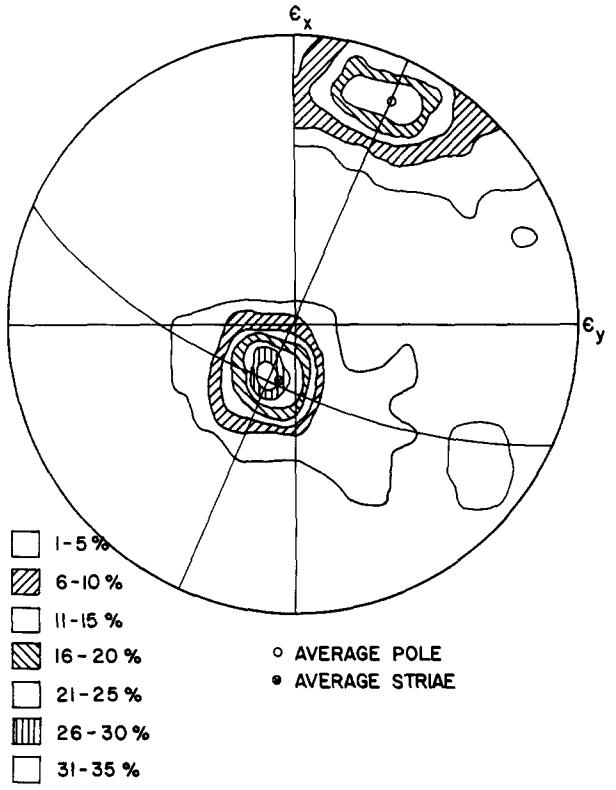

Fig. 15. Contoured stereonet plot of fault poles and striations, after correction for tilt and declination and reflection into the northeast quadrant using rules of orthorhombic symmetry. The strong maximum of striations lies exactly down dip, as the odd axis model predicts. Contour intervals are per one per cent area.

fault slip to fault spacing must be calculated. A rough estimate of the value of R for Chimney Rock array can be made by dividing the mean of the average slip on the major faults (Fig. 13), 14.4 m, by the average distance between the faults of the same set, 291 m (determined by measuring the distances between adjacent faults of the same set on a detailed map of the Chimney Rock array), which yields a value of 0.05 for R. Comparing the average fault slip and spacing values for individual traverses yields R values of 0.02–0.04. Therefore, the simplified odd-axis model equations (27)–(29) can be applied with confidence.

Table 2. Predicted and observed geometric and kinematic parameters for the Chimney Rock fault array

$\alpha = 24°$, $\delta = 72°$, $R = 0.025$ Predicted	Observed (average)	Observed (maximum)
$\varepsilon_{sim} = 0.024$ $\varepsilon_{int} = 0.0049$ $\varepsilon_{odd} = -0.029$	$\varepsilon_x = 0.0041$ $\varepsilon_y = 0.0007$ $\varepsilon_z = -0.0048$	$\varepsilon_x = 0.0066$ $\varepsilon_y = 0.0012$ $\varepsilon_z = -0.0078$
$\frac{\varepsilon_{int}}{\varepsilon_{sim}} = \tan^2 \alpha = 0.20$	$\frac{\varepsilon_y}{\varepsilon_x} = 0.17$	$\frac{\varepsilon_y}{\varepsilon_x} = 0.18$
$\frac{\varepsilon_{int}}{\varepsilon_{odd}} = -\sin^2 \alpha = -0.16$	$\frac{\varepsilon_y}{\varepsilon_z} = -0.15$	$\frac{\varepsilon_y}{\varepsilon_z} = -0.15$
$\frac{\varepsilon_{sim}}{\varepsilon_{odd}} = -\cos^2 \alpha = -0.84$	$\frac{\varepsilon_x}{\varepsilon_z} = -0.85$	$\frac{\varepsilon_x}{\varepsilon_z} = -0.85$
$k_{predicted} = -0.16$	$k_{observed} = -0.15$	
Fault encounter ratio: $\tan \alpha = 0.45$	$n_y/n_x = 0.41$	

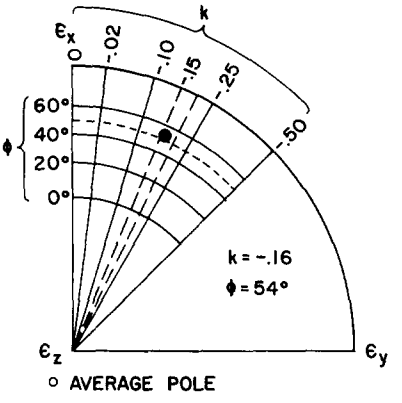

Fig. 16. Mean reflected fault pole from Fig. 15 plotted on the slip model net for normal faults ($k < 0$) (Reches 1983). The mean pole predicts $k = -0.16$.

Table 2 lists the three predicted principal extension ratios calculated using $\alpha = 24°$, along with the observed ratios based on the measured principal extension values given in Table 1. The predicted ratio of horizontal extension ($\varepsilon_y/\varepsilon_x$) equals 0.20, very close to the observed ratios of 0.17 for the average observed extension values and 0.18 for the maximum observed values. The other ratios are even closer, as $\varepsilon_y/\varepsilon_z$ predicted equals -0.16 while $\varepsilon_y/\varepsilon_z$ observed is -0.15, and $\varepsilon_x/\varepsilon_z$ predicted equals -0.84 while $\varepsilon_x/\varepsilon_z$ observed is -0.85. Table 2 also includes the value of k predicted by the slip model (Fig. 16), -0.16, which is quite close to the observed value of $\varepsilon_y/\varepsilon_z$, -0.15.

Although the unequal populations of the four fault sets makes the Chimney Rock array less than ideal, another parameter can be used to check the application of the odd-axis model. The expected ratio of fault encounters in the principal horizontal directions is given by the ratio of equations (14) and (15):

$$\frac{n_{int}}{n_{sim}} = \frac{\sin \alpha}{\cos \alpha} = \tan \alpha. \quad (38)$$

Table 2 contains the predicted (0.45) and observed (0.41) ratios of fault encounters in the horizontal directions, the latter based on the horizontal strain traverses. The close agreement again reflects the true orthorhombic nature of the Chimney Rock array and supports the application of the theoretical models.

DISCUSSION AND CONCLUSIONS

The excellent agreement between predicted and observed geometric and kinematic parameters at Chimney Rock reveals the true orthorhombic nature of the fault system, while providing a showcase for the use of the fault models in the field. The Chimney Rock array clearly represents the results of faulting in a three-dimensional strain field with a near-vertical odd axis. The maximum concentration of striations on the fault surfaces lies exactly down dip as predicted, and the predicted and observed ratios of principal extension agree closely.

The odd-axis model provides a simple method for identifying and locating the principal strain axes, assuming orthorhombic symmetry and coaxial strain. Equations relate principal extensions and ratios to fault plane orientations and ratios of average fault slip to average fault spacing. For small ratios of fault slip to spacing, the odd-axis model equations are elementary functions of fault 'strike' only.

The odd-axis model expresses the same relationships as Reches' slip model. These complimentary models provide a framework for dealing with multiple (orthorhombic) fault sets developed in three-dimensional strain fields. Both models also suggest that the conjugate faults of Anderson (1951) represent a special case of plane-strain deformation. Orthorhombic faults and these theoretical models represent at least a step closer to a more general scheme of faulting.

Acknowledgements—The development of the odd-axis model and of this manuscript was aided greatly by discussions with Ze'ev Reches, George Davis, Stephen Naruk, Clement Chase and Shirlee Krantz. Additional helpful comments were made by Ann Bykerk-Kauffman and William Dickinson. I wish to thank Ronald L. Bruhn and an anonymous reviewer. Shirlee Krantz, Susanne Janecke, Stephen Naruk and Barrie Bernstein provided valuable field assistance. This project was funded by Standard Oil Production Company (SOHIO) and the Laboratory of Geotectonics at the University of Arizona.

REFERENCES

Anderson, E. M. 1951. *The Dynamics of Faulting*. Oliver and Boyd, London.

Arthaud, F. 1969. Methode de determination graphique des directions de raccourcissement, d'allongement et intermediaire d'une population de failles. *Bull. Soc. geol. Fr.* **11**, 729–737.

Aydin, A. & Reches, Z. 1982. Number and orientations of fault sets in the field and in experiments. *Geology* **10**, 110–112.

Cass, J. T. 1955. Photogeologic map of the Desert Lake-9 Quadrangle, Emery County, Utah. United States Geological Survey Miscellaneous Investigations Map I-103.

Gilluly, J. 1928. Geology and oil and gas prospects of the San Rafael Swell, Utah. *Contr. econ. Geol.* 69–130.

Hobbs, B. E., Means, W. D. & Williams, P. F. 1976. *An Outline of Structural Geology*. John Wiley and Sons, New York.

Krantz, R. W. 1986. Orthorhombic fault patterns and three-dimensional strain analysis, northern San Rafael Swell, Utah (abs.). *Geol. Soc. Am. Abs. w. Prog.* **18**, 125.

Oertel, G. 1965. The mechanics of faulting in clay experiments. *Tectonophysics* **2**, 343–393.

Orkid, P. P. 1954. Photogeologic map of the Desert Lake-8 Quadrangle, San Juan and Garfield Counties, Utah. United States Geological Survey Miscellaneous Investigations Map I-4.

Orkid, P. P. 1955. Photogeologic map of the Woodside-5 Quadrangle, Emery County, Utah. United States Geological Survey Miscellaneous Investigations Map I-5.

Ramsay, J. G. 1967. *Folding and Fracturing of Rocks*. McGraw-Hill, New York.

Reches, Z. 1978. Analysis of faulting in a three-dimensional strain field. *Tectonophysics* **47**, 109–129.

Reches, Z. 1983. Faulting of rocks in three-dimensional strain fields II. Theoretical analysis. *Tectonophysics* **95**, 133–156.

Reches, Z. & Dieterich, J. H. 1983. Faulting of rocks in three-dimensional strain fields I. Failure of rocks in polyaxial, servo-controlled experiments. *Tectonophysics* **95**, 111–132.

APPENDIX A

The following equations, modified from Reches (1983), express the orientations of the poles to the preferred faults, **N**, and the slip vectors, **S**, as functions of the ratio of intermediate to minimum extension, k, and the internal friction angle, ϕ. Each orientation is given as three direction cosines with respect to the principal strain axes, $\varepsilon_x \geq \varepsilon_y \geq \varepsilon_z$. The four fault set orientations and associated slip vectors are generated by using the sign permutations listed below.

For $k > 0$:
$$N_x = (\sqrt{2}/2)(1 + \sin\phi)^{1/2}$$
$$N_y = \tfrac{1}{2}(2k/1 + k)^{1/2}(1 + \sin\phi)^{1/2}$$
$$N_z = \tfrac{1}{2}(2/1 + k)^{1/2}(1 - \sin\phi)^{1/2}$$
$$S_x = (\sqrt{2}/2)(1 - \sin\phi)^{1/2}$$
$$S_y = \tfrac{1}{2}(2k/1 + k)^{1/2}(1 + \sin\phi)^{1/2}$$
$$S_z = \tfrac{1}{2}(2/1 + k)^{1/2}(1 + \sin\phi)^{1/2}.$$

For $k < 0$:
$$N_x = (\sqrt{2}/2)(1 + k)^{1/2}(1 + \sin\phi)^{1/2}$$
$$N_y = (\sqrt{2}/2)(-k)^{1/2}(1 + \sin\phi)^{1/2}$$
$$N_z = (\sqrt{2}/2)(1 - \sin\phi)^{1/2}$$
$$S_x = (\sqrt{2}/2)(1 + k)^{1/2}(1 - \sin\phi)^{1/2}$$
$$S_y = (\sqrt{2}/2)(-k)^{1/2}(1 - \sin\phi)^{1/2}$$
$$S_z = (\sqrt{2}/2)(1 + sin\,\phi)^{1/2}.$$

Fault set 1: N_x, N_y, and N_z; S_x, S_y, and S_z.
Fault set 2: N_x, $-N_y$, and N_z; S_x, $-S_y$, and S_z.
Fault set 3: N_x, $-N_y$, and $-N_z$; S_x, $-S_y$, and $-S_z$.
Fault set 4: N_x, N_y, and $-N_z$; S_x, S_y, and $-S_z$.

APPENDIX B

Based on the geometric relationships inherent in the slip model of Reches (1983), the pole to any orthorhombic fault set, **N**, the slip vector for that set, **S**, and the odd axis must be coplanar.

For $k < 0$, $\boldsymbol{\epsilon}_z$ is the odd axis. **N**, **S** and $\boldsymbol{\epsilon}_z$ are coplanar if and only if their triple scalar product is zero, that is,

$$\mathbf{N}\cdot(\mathbf{S} \times \boldsymbol{\epsilon}_z) = 0. \tag{B1}$$

N, **S**, and $\boldsymbol{\epsilon}_z$ can be expressed as unit vectors:

$$\mathbf{N} = (N_x, N_y, N_z); \tag{B2}$$

$$\mathbf{S} = (S_x, S_y, S_z); \tag{B3}$$

$$\boldsymbol{\epsilon}_z = (0, 0, 1). \tag{B4}$$

Since

$$\mathbf{N}\cdot(\mathbf{S} \times \boldsymbol{\epsilon}_z) = \begin{vmatrix} N_x & N_y & N_z \\ S_x & S_y & S_z \\ 0 & 0 & 1 \end{vmatrix} \tag{B5}$$

then

$$\mathbf{N}\cdot(\mathbf{S} \times \boldsymbol{\epsilon}_z) = (1)(-1)\begin{vmatrix} N_x & N_y \\ S_x & S_y \end{vmatrix} = N_xS_y - N_yS_x. \tag{B6}$$

Substituting from Appendix A yields:

$$\mathbf{N}\cdot(\mathbf{S} \times \boldsymbol{\epsilon}_z) = \tfrac{1}{2}(1 + k)^{1/2}(-k)^{1/2}(1 + \sin\phi)^{1/2}(1 - \sin\phi)^{1/2} - \tfrac{1}{2}(1 + k)^{1/2}(-k)^{1/2}(1 + \sin\phi)^{1/2}(1 - \sin\phi)^{1/2} \tag{B7}$$

or

$$\mathbf{N}\cdot(\mathbf{S} \times \boldsymbol{\epsilon}_z) = 0.$$

Therefore, **N**, **S** and $\boldsymbol{\epsilon}_z$ are coplanar.

A similar proof can be constructed for $k > 0$ where $\boldsymbol{\epsilon}_x$ is the odd axis.